

The method of Gaussian weighted trajectories.

V. On the 1GB procedure for polyatomic processes

*L. Bonnet**

*Institut des Sciences Moléculaires, Université Bordeaux 1,
351 Cours de la Libération, 33405 Talence Cedex, France*

J. Espinosa-Garcia

Departamento de Química Física, Universidad de Extremadura, 06071 Badajoz Spain.

In recent years, many chemical reactions have been studied by means of the quasi-classical trajectory (QCT) method within the Gaussian binning (GB) procedure. The latter consists in "quantizing" the final vibrational actions in Bohr spirit by putting strong emphasis on the trajectories reaching the products with vibrational actions close to integer values. A major drawback of this procedure is that if N is the number of product vibrational modes, the amount of trajectories necessary to converge the calculations is $\sim 10^N$ larger than with the standard QCT method. Applying it to polyatomic processes is thus problematic. In a recent paper, however, Czako and Bowman propose to quantize the total vibrational energy instead of the vibrational actions [G. Czako and J. M. Bowman, *J. Chem. Phys.*, 131, 244302 (2009)], a procedure called 1GB here. The calculations are then only ~ 10 times more time-consuming than with the standard QCT method, allowing thereby for considerable numerical saving. In this paper, we propose some theoretical arguments supporting the 1GB procedure and check its validity on model test cases as well as the prototype four-atom reaction $\text{OH} + \text{D}_2 \rightarrow \text{HOD} + \text{D}$.

I. INTRODUCTION

Improving our ability to accurately describe gas-phase chemical reactions and inelastic collisions is a stimulating theoretical issue at the interface of physics and chemistry [1] and a necessary step towards a deep understanding of the evolution of planetary atmospheres

* Corresponding author. Email: l.bonnet@ism.u-bordeaux1.fr

and interstellar clouds.

Assuming that for a given process, the electronic problem has been solved [2], i.e., the potential energy of interaction between nuclei is known, nuclear motions can be studied either quantum [3–10] or classical mechanically [11, 12]. For the present time, however, quantum scattering approaches can hardly be applied to more than three-atom processes, despite current computer performances and a great deal of methodological effort made to go beyond the triatomic problem [13–17].

On the other hand, the classical approach, well known as the quasi-classical trajectory method (QCTM) [11, 12], is much less time consuming and can therefore be applied to almost any process, independently on the number of atoms involved. We focus our attention on this method in the present paper.

A major goal of QCTM is to predict the distributions of the translational energy between bimolecular collision or photodissociation products as well as the distribution of their quantum states [1]. These distributions, measured in molecular beam experiments, are among the most refined data on chemical reactivity and molecular reaction dynamics. In this work, we concentrate on the possible descriptions of these two quantities within QCTM.

In its standard implementation, QCTM deals with the *standard binning* (SB) procedure (or histogram method) for assigning trajectories to the various quantum states available. In order to introduce this procedure, we consider the three-atom exchange reaction of the type $A + BC \longrightarrow AB + C$. If at the end of a given reactive trajectory, the vibrational action of AB is x in units of h (see appendix A for the mathematical definition of x) and its rotational angular momentum is j in units of \hbar , the trajectory is assumed to only contribute to the AB quantum state (\bar{x}, \bar{j}) where \bar{x} and \bar{j} are the nearest integers of x and j respectively (in the following, the nearest integer of any variable will also be denoted by the variable with a bar on top of it).

About ten years ago, however, it was suggested that such a procedure might lead to wrong predictions when the energy available to the products is too low for the quantum and classical densities of product states to be equal, or equivalently, when the available quantum states are widely spaced as compared to the energy disposal [18]. A *Gaussian Binning* (GB) procedure was then proposed [18] which amounts to assigning to each trajectory a Gaussian statistical weight such that the closer the final actions to their nearest integers, the larger the weight (by action, we mean here both vibrational actions and rotational

angular momenta in the previously defined units). For the previous triatomic process, the Gaussian weight of the trajectory ending with (x, j) is

$$G(x, j) = G(x - \bar{x})G(j - \bar{j}) \quad (1)$$

with

$$G(u) = \frac{e^{-u^2/\epsilon^2}}{\pi^{1/2}\epsilon}, \quad (2)$$

ϵ being usually kept at ~ 0.05 [19–21]. Like in the SB procedure, trajectories do only contribute to the quantum state defined by the center (\bar{x}, \bar{j}) of the bin or unit square in which (x, j) stands. The GB procedure is therefore a practical way of taking into account Bohr quantization in the analysis of the final results. The GB procedure turns out to be a reminiscence of the use of narrow boxes proposed by Ron *et al* in the early 80's [22], a method apparently ignored or forgotten by QCTM users.

Initially proposed on the basis of intuitive arguments, the GB procedure was later shown to be a practical implementation of classical S matrix theory (CSMT) in the random phase approximation [23, 24], CSMT being the first and simplest (or least complex) semi-classical approach of molecular collisions pioneered by Miller and Marcus in the early seventies [25–31].

The Gaussian weight $G(u)$ is characterized by a full width at half maximum of ~ 10 percent. This means that the values of x and j respectively in the ranges $[\bar{x} - 0.05, \bar{x} + 0.05]$ and $[\bar{j} - 0.05, \bar{j} + 0.05]$ mostly contribute to the GB population of the level (\bar{x}, \bar{j}) , as compared with the values in the unit ranges $[\bar{x} - 0.5, \bar{x} + 0.5]$ and $[\bar{j} - 0.5, \bar{j} + 0.5]$ which contribute to the SB population. Therefore, the area in the (x, j) plane contributing to the GB population is ~ 100 times smaller than the one contributing to the SB population and it is necessary to run ~ 100 times more trajectories within the GB procedure than within the SB one for the same level of convergence of the final results.

In many experiments, however, the number of available rotational states of AB is significantly larger than the number of its vibrational states (more than ~ 10 against less than ~ 3) and one arrives at the same result when weighting the trajectories by Eq. (1) or by $G(x - \bar{x})$ alone. Within this partial GB procedure, corresponding to Eqs. (13) and (14) of reference 24, it is thus sufficient to run ~ 10 times more trajectories than within the HB

one [19–21, 24, 32–35].

However, considering polyatomic reactions where the number of vibrational modes is easily ten or more, strongly clouds the situation. The reason is that "quantizing" N modes amounts to weight the trajectories by a product of N Gaussians. Therefore, one is led to run $\sim 10^N$ times more trajectories within the GB procedure than within the SB one. For the reaction $F+CH_4 \rightarrow FH+CH_3$ and its isotopic variants, much studied experimentally in the recent years [36], the previous number is ~ 10 millions ! Since one needs at least a few hundreds of thousands of trajectories within the HB procedure, one should run a few trillions of trajectories within the GB procedure, which is just not feasible.

In order to circumvent this difficulty, Czako and Bowman recently proposed to weight the trajectories by $G(u)$ (see Eq. (2)) with

$$u = \frac{\sum_{i=1}^N \omega_i (x_i - \bar{x}_i)}{\sum_{i=1}^N \omega_i}, \quad (3)$$

x_i being the vibrational action for the i^{th} mode and ω_i the corresponding frequency [37]. In other words, they proposed to quantize, with one Gaussian only, the total vibrational energy (in the harmonic approximation) instead of the vibrational actions. Consequently, this 1GB procedure allows for a huge amount of computational savings for large systems.

The goal of the present paper is to propose theoretical arguments supporting this procedure and check its validity on model as well as actual processes.

The paper is organized as follows. In section II, the 1GB procedure is shown to be equivalent to the usual GB procedure for statistical collinear processes. We then discuss the conditions for its validity in the general case. The predictions to which it leads are compared in section III with the usual SB and GB predictions for a model test case involving three vibrational modes. In section IV, the approach is applied to the prototype four-body chemical reaction $OH+D_2 \rightarrow HOD+D$ which is among the simplest polyatomic bimolecular reactions [38–44]. We finally conclude in section V.

II. THEORETICAL ANALYSIS OF THE 1GB PROCEDURE

In a first step, we focus our attention on collinear processes in the course of which nuclei keep on a line fixed in the laboratory frame. The realistic three-dimensional case where

rotation motions are active is considered in a second step.

A. Collisional system involving two vibrational modes

Consider the collinear inelastic collision between atom A and the triatomic molecule BCD at the classically available energy E with respect to the free fragments. Assuming that the harmonic approximation is valid for the intra-molecular motion of BCD, its vibrational energy E_V at the end of the collision reads (see appendix A)

$$E_V = \omega_1(x_1 + \frac{1}{2}) + \omega_2(x_2 + \frac{1}{2}) \tag{4}$$

where ω_1 and ω_2 are the energy spacings between neighboring states for the two vibrational stretching normal modes of BCD and x_1 and x_2 are their related actions (since B, C and D are aligned, the usual bending vibration is ignored).

The relative translational energy E_T between A and BCD satisfies the identity

$$E_T = E - E_V. \tag{5}$$

We call $\rho(x_1, x_2)$ the classical distribution of the actions x_1 and x_2 , supposed to be normalized to unity.

Additional paragraph 1:

We shall consider the formal expressions of both the translational energy distribution of the final products and the one of their quantum states. However, we shall only represent the former distribution in the figures. We might have done the contrary, but the translational energy distribution is by far the most widely measured in molecular beam experiments. We thus believe that discussing the different ways this distribution can be represented in QCT studies is an important issue. In addition to that, the translational and internal energies being mathematically related (see Eq. (5)), the two distributions can, in principle, be deduced from each other. In this section and the next one, for instance, it will turn out that the product state distribution is readily obtained from visual inspection

of the translational energy distribution.

End of the additional paragraph 1.

B. Purely classical translational energy distribution

The translational energy distribution obtained from a strict application of classical mechanics reads

$$P_C(E_T) = \int dx_1 dx_2 \rho(x_1, x_2) \delta(E_T - E + \omega_1(x_1 + \frac{1}{2}) + \omega_2(x_2 + \frac{1}{2})) \quad (6)$$

(see appendix B for its derivation). Since this density has no quantum attribute, it is usually in bad agreement with quantum scattering and/or highly resolved experimental distributions, unless E is much larger than the average quantum level spacing.

Additional paragraph 2:

Nevertheless, this distribution has been so widely used in QCT studies that for the sake of completeness, we shall be considering it in this work.

End of the additional paragraph 2.

C. SB distributions

A variant of the previous distribution, incorporating to some extent the idea of vibrational quantization, is as follows:

$$P_{SB}(E_T) = \int dx_1 dx_2 \rho(x_1, x_2) \delta(E_T - E + \omega_1(\bar{x}_1 + \frac{1}{2}) + \omega_2(\bar{x}_2 + \frac{1}{2})). \quad (7)$$

We note that the only difference with respect to Eq. (6) is that the x_i 's in the delta function have been replaced by the \bar{x}_i 's.

As in the SB procedure, the bins are one unit wide, the domain of integration in Eq. (7) consists of the domains corresponding to each pair of the integer quantum numbers n_1 and n_2 . Decomposing the integral in (7) into a sum of integrals over these unit-sized domains, one gets:

$$P_{SB}(E_T) = \sum_{n_1, n_2} \int_{D_{n_1 n_2}} dx_1 dx_2 \rho(x_1, x_2) \delta(E_T - E + \omega_1(\bar{x}_1 + \frac{1}{2}) + \omega_2(\bar{x}_2 + \frac{1}{2})) \quad (8)$$

where $D_{n_1 n_2}$ is the unit square in the plane (x_1, x_2) centered on (n_1, n_2) . The \bar{x}_i 's being equal to the n_i 's in $D_{n_1 n_2}$, we then arrive at

$$P_{SB}(E_T) = \sum_{n_1, n_2} P_{SB}(n_1, n_2) \delta(E_T - E + \omega_1(n_1 + \frac{1}{2}) + \omega_2(n_2 + \frac{1}{2})) \quad (9)$$

where

$$P_{SB}(n_1, n_2) = \int_{D_{n_1 n_2}} dx_1 dx_2 \rho(x_1, x_2) \quad (10)$$

is recognized to be the SB population of the quantum state (n_1, n_2) .

D. GB distribution

The GB distribution is readily found from Eqs. (9) and (10) to be given by

$$P_{GB}(E_T) = \sum_{n_1, n_2} P_{GB}(n_1, n_2) \delta(E_T - E + \omega_1(n_1 + \frac{1}{2}) + \omega_2(n_2 + \frac{1}{2})) \quad (11)$$

and

$$P_{GB}(n_1, n_2) = \int_{D_{n_1 n_2}} dx_1 dx_2 G(x_1, x_2) \rho(x_1, x_2) \quad (12)$$

with

$$G(x_1, x_2) = G(x_1 - n_1)G(x_2 - n_2). \quad (13)$$

The even unit weight in the integrand of Eq. (10) has thus been replaced by the Gaussian weight $G(x_1, x_2)$.

When making ϵ tend to zero, we arrive at a distribution which we shall call "exact" in the following. It is of course not exact in the true quantum mechanical sense, but it is the best distribution we can arrive at by simple inclusion of Bohr quantization in QCTM. In this limit, $G(u)$ tends to the delta-function $\delta(u)$ and Eq. (12) reads

$$P_E(n_1, n_2) = \int_{D_{n_1 n_2}} dx_1 dx_2 \delta(x_1 - n_1) \delta(x_2 - n_2) \rho(x_1, x_2), \quad (14)$$

giving immediately

$$P_E(n_1, n_2) = \rho(n_1, n_2). \quad (15)$$

Then, Eq. (11) reads

$$P_E(E_T) = \sum_{n_1, n_2} \rho(n_1, n_2) \delta(E_T - E + \omega_1(n_1 + \frac{1}{2}) + \omega_2(n_2 + \frac{1}{2})). \quad (16)$$

Since the 1GB distribution to be derived in the next section is supposed to be an alternative to the GB one, the former will be systematically tested against the latter and its "exact" limit in the followings.

E. 1GB distributions

1. Statistical case

Indirect chemical reactions involving long-lived complexes have been the subject of intense research during the last few years [45–50].

Additional paragraph 3:

In Phase Space Theory, the simplest statistical approach (see references [46] and [50] and references therein), the final product states consistent with total energy and total angular momentum are equally probable.

End of the additional paragraph 3.

For the present system, the analogous situation corresponds to a uniform density $\rho(x_1, x_2)$ in the energetically available action space defined by

$$E \geq \omega_1(x_1 + \frac{1}{2}) + \omega_2(x_2 + \frac{1}{2}) \tag{17}$$

and both x_1 and x_2 greater than minus 1/2. This triangular domain is represented in Fig. 1 for E , ω_1 and ω_2 kept at 5.2, 1 and 2.3 respectively ; these values have been chosen in such a way that six quantum states, indicated by red dots, are available (different values might have been chosen as well). Three forbidden quantum states are represented by dark blue dots and three unit squares centered on quantum states are emphasized. The two salmon ones correspond to available quantum states while the light blue one corresponds to a forbidden state.

Throughout the present part, $\rho(x_1, x_2)$ will be simply denoted ρ . Its value is

$$\rho = \frac{2\omega_1\omega_2}{E^2} \tag{18}$$

(the inverse of the area of the green triangle) inside the triangle and zero outside.

$P_C(E_T)$ can be determined analytically by using the identity

$$\delta(ax) = \frac{1}{|a|}\delta(x), \tag{19}$$

leading to

$$P_C(E_T) = \frac{2}{E} \left(1 - \frac{E_T}{E}\right). \tag{20}$$

Additional paragraph 4:

In principle, the translational energy distribution measured in a perfect experiment

would consist in a set of Dirac delta functions for the energies complementary with those of the allowed product quantum states. However, no experiment is "perfect". There is always an uncertainty in both the total energy available to the products and the measure of the translational energy. Consequently, the peaks are necessarily broaden. In order to take into account this uncertainty in the theory, we shall replace the Dirac peaks present in Eqs. (9), (11) and (16) by $G(u)$ (see Eq. (2)) with $\epsilon = 0.05$, meaning that the uncertainty on E_T is ~ 0.1 . This arbitrary value of ϵ makes the peaks neither too narrow, nor too broad as compared to the total energy E . The fact that it was kept at the same value as in the GB procedure should not confuse the reader. Its choice was a matter of convenience, nothing else.

It is worth emphasizing that there are thus two separate issues in this work: the first, and central one, is the use of Gaussians to deal with Bohr quantization in QCT calculations ; the second, and minor one, is the use of Gaussians to take into account the uncertainty in the measurement of the translational energy.

End of the additional paragraph 4.

$P_{SB}(E_T)$ and $P_{GB}(E_T)$ were determined by Monte-Carlo integration over x_1 and x_2 , using $N_T = 200000$ points randomly chosen in the triangular domain. The corresponding expressions are

$$P_X(E_T) = \sum_{n_1, n_2} P_X(n_1, n_2) G(E_T - E + \omega_1(n_1 + \frac{1}{2}) + \omega_2(n_2 + \frac{1}{2})) \quad (21)$$

where X stands for SB or GB , with

$$P_{SB}(n_1, n_2) = \frac{N_{D_{n_1 n_2}}}{N_T}, \quad (22)$$

$N_{D_{n_1 n_2}}$ being the number of trajectories ending in $D_{n_1 n_2}$, and

$$P_{GB}(n_1, n_2) = \frac{1}{N_T} \sum_{k=1}^{N_{D_{n_1 n_2}}} G(x_1^k, x_2^k), \quad (23)$$

x_1^k and x_2^k being the final actions for the k^{th} trajectory ending in $D_{n_1 n_2}$.

The four distributions are represented in Fig. 2 for 500 values of E_t regularly distributed between 0 and E .

$P_C(E_T)$ appears to be in complete disagreement with the "benchmark" distribution $P_E(E_T)$, for by construction, no structure can be reproduced. $P_{SB}(E_T)$ takes the structures into account, but the heights of the peaks are inaccurate for the small values of E_T . Conversely, $P_{GB}(E_T)$ is in excellent agreement with $P_E(E_T)$, as expected. Note that for these two distributions, the peaks have the same height, meaning that the populations of the available quantum states are all equal, in agreement with the statistical hypothesis.

The heights of the peaks of $P_{SB}(E_T)$ increase with E_t . This can be easily understood from Fig. 1. The values of the translational energies corresponding to the top of the peaks (see Fig. 2) are given by

$$E_{n_1 n_2} = E - \left(\omega_1 \left(n_1 + \frac{1}{2} \right) + \omega_2 \left(n_2 + \frac{1}{2} \right) \right), \quad (24)$$

the integers n_1 and n_2 being such that (n_1, n_2) is an allowed quantum state. These states are $(1, 1)$, $(3, 0)$, $(0, 1)$, $(2, 0)$, $(1, 0)$ and $(0, 0)$, by order of increasing translational energy. The straight lines defined by

$$\omega_1 \left(x_1 + \frac{1}{2} \right) + \omega_2 \left(x_2 + \frac{1}{2} \right) = E - E_{n_1 n_2} \quad (25)$$

are represented in Fig. 1. Clearly, the spacings between these lines exactly follow the spacings between the nearest $E_{n_1 n_2}$'s (see Fig. 2).

Now, the heights are proportional to the SB populations, themselves proportional to the available areas of the unit squares centered on the quantum states. From Fig. 1, it is clear that for $(0, 0)$, this area, represented in salmon, is 1, but for $(1, 1)$, it is only equal to ~ 0.6 . One also guesses that for $(3, 0)$ and $(0, 1)$, the areas are equal to ~ 0.7 and ~ 0.9 respectively while for the remaining states $(1, 0)$ and $(2, 0)$, they are equal to ~ 1 . This explains why the heights of the first three peaks of $P_{SB}(E_T)$ (see Fig. 2) are only ~ 60 , ~ 70 and ~ 90 percent of the height of the remaining peaks. This cannot happen with the GB distribution,

for with sufficiently thin Gaussians, their value is the same for all the quantum states.

Having defined the system of interest and applied the different methods currently utilized in QCT calculations today, we are now in a position to introduce the 1GB procedure. $P_E(n_1, n_2)$, given by Eq. (14) with $\rho(x_1, x_2) = \rho$, can be rewritten as

$$P_E(n_1, n_2) = \rho \int_{D_{n_1 n_2}} dy_1 dy_2 \delta(y_1) \delta(y_2) \quad (26)$$

where y_1 and y_2 are two new coordinates related to x_1 and x_2 by the rotation

$$y_1 = \cos\theta (x_1 - n_1) - \sin\theta (x_2 - n_2) \quad (27)$$

and

$$y_2 = \sin\theta (x_1 - n_1) + \cos\theta (x_2 - n_2) \quad (28)$$

with

$$\cos\theta = \frac{\omega_2}{(\omega_1^2 + \omega_2^2)^{1/2}} \quad (29)$$

and

$$\sin\theta = \frac{\omega_1}{(\omega_1^2 + \omega_2^2)^{1/2}}. \quad (30)$$

The axis y_1 runs through (n_1, n_2) and is parallel to the hypotenuse of the green triangle. y_1 is thus one of the red axes represented in Fig. 1. The axis y_2 also runs through (n_1, n_2) and is orthogonal to y_1 . These axes are represented in Fig. 3 as well as the unit square $D_{n_1 n_2}$. It is clear that integration over y_1 and y_2 in Eq. (26) immediately leads to Eq. (15).

Let us now define the population

$$P'_E(n_1, n_2) = \alpha \rho \int_{D_{n_1 n_2}} dy_1 dy_2 \delta(y_2) \quad (31)$$

where

$$\alpha = \max(\cos\theta, \sin\theta). \quad (32)$$

As compared with Eq. (26), Eq. (31) involves only one Dirac distribution. After a trivial integration with respect to y_2 , $P'_E(n_1, n_2)$ reads

$$P'_E(n_1, n_2) = \alpha \rho \int_{D_{n_1 n_2}} dy_1. \quad (33)$$

However, one deduces from Fig. 3, corresponding to the case where $\cos\theta$ is greater than $\sin\theta$ (θ lower than $\pi/4$), that

$$\cos\theta = \frac{1}{\int_{D_{n_1 n_2}} dy_1}. \quad (34)$$

In the same way, it can be easily shown that when $\cos\theta$ is smaller than $\sin\theta$,

$$\sin\theta = \frac{1}{\int_{D_{n_1 n_2}} dy_1}. \quad (35)$$

α , given by Eq. (32), can thus be rewritten as

$$\alpha = \frac{1}{\int_{D_{n_1 n_2}} dy_1}, \quad (36)$$

and Eq. (33) leads to

$$P'_E(n_1, n_2) = \rho. \quad (37)$$

We thus arrive at the conclusion that the $P'_E(n_1, n_2)$'s are equal to the $P_E(n_1, n_2)$'s (see Eq. (15)). Consequently, $P_E(n_1, n_2)$ can be rewritten from Eqs. (28)-(31) as

$$P_E(n_1, n_2) = \alpha \int_{D_{n_1 n_2}} dy_1 dy_2 \delta\left(\frac{\omega_1 (x_1 - n_1) + \omega_2 (x_2 - n_2)}{(\omega_1^2 + \omega_2^2)^{1/2}}\right) \rho. \quad (38)$$

Moreover, from Eqs. (29), (30) and (32) and using the fact that $\alpha\delta(q) = \delta(q/\alpha)$ (deduced from Eq. (19)), we obtain

$$P_E(n_1, n_2) = \int_{D_{n_1 n_2}} dy_1 dy_2 \delta\left(\frac{\omega_1 (x_1 - n_1) + \omega_2 (x_2 - n_2)}{\max(\omega_1, \omega_2)}\right) \rho. \quad (39)$$

Applying the GB procedure, i.e. replacing δ by G , and going back to the x_i 's, $P_E(n_1, n_2)$

finally reads

$$P_{1GB}(n_1, n_2) = \int_{D_{n_1 n_2}} dx_1 dx_2 G\left(\frac{\omega_1 (x_1 - n_1) + \omega_2 (x_2 - n_2)}{\max(\omega_1, \omega_2)}\right) \rho(x_1, x_2), \quad (40)$$

an expression formally close to the expression

$$P_{1GB}(n_1, n_2) = \int_{D_{n_1 n_2}} dx_1 dx_2 G\left(\frac{\omega_1 (x_1 - n_1) + \omega_2 (x_2 - n_2)}{\omega_1 + \omega_2}\right) \rho(x_1, x_2) \quad (41)$$

corresponding to the calculations of Czako and Bowman [37].

$P_{1GB}(E_t)$ is then deduced from $P_{1GB}(n_1, n_2)$ by

$$P_{1GB}(E_T) = \sum_{n_1, n_2} P_{1GB}(n_1, n_2) \delta(E_T - E + \omega_1(n_1 + \frac{1}{2}) + \omega_2(n_2 + \frac{1}{2})). \quad (42)$$

Like previously, the δ function in the above expression is replaced by a Gaussian in order to take into account the uncertainty in the measurement of the translational energy. Moreover, the Monte-Carlo expression of $P_{1GB}(n_1, n_2)$ reads

$$P_{1GB}(n_1, n_2) = \frac{1}{N_T} \sum_{k=1}^{N_{D_{n_1 n_2}}} G\left(\frac{\omega_1 (x_1^k - n_1) + \omega_2 (x_2^k - n_2)}{\omega}\right), \quad (43)$$

with

$$\omega = \max(\omega_1, \omega_2) \quad (44)$$

according to Eq. (40) or

$$\omega = \omega_1 + \omega_2 \quad (45)$$

according to Eq. (41). Eqs. (2), (43) and (45) correspond to Eqs. 13 and 16 in the paper by Czako and Bowman [37]. The distribution obtained from Eqs. (42)-(44) is represented in Fig. 4 (1GB curve), together with $P_E(E_T)$ (like previously, ϵ was kept at 0.05 for all the Gaussians). The two densities are in such a good agreement that they cannot be distinguished. On the other hand, the distribution obtained from Eqs. (42), (43) and (45), also shown in Fig. 4 (1GB' curve), has the good shape, but its norm is too large. We shall come back to this important normalization issue in section II.H.

Additional paragraph 5:

One may wonder whether the selection of y_2 to be the argument of the delta function in Eq. (31) is arbitrary. For instance, one might be tempted by stating in view of Fig. 3 that interchanging y_1 and y_2 still leads to the equality between $P_E(n_1, n_2)$ and $P'_E(n_1, n_2)$. This is indeed true for the less excited states $(0, 0)$, $(1, 0)$, $(2, 0)$ and $(0, 1)$, but not for the most excited states $(3, 0)$ and $(1, 1)$ (see Fig. 1). As a matter of fact, the upper limit of the green triangle would limit the integration along the new y_1 axis (corresponding to the y_2 axis in Fig. 3) in such a way that for $(3, 0)$ and $(1, 1)$, $P'_E(n_1, n_2)$ would be lower than $P_E(n_1, n_2)$. On the other hand, slightly varying θ about the value defined by Eqs. (29) and (30) will preserve the equality between $P_E(n_1, n_2)$ and $P'_E(n_1, n_2)$ provided that the hypotenuse of the green triangle is not too close to the most excited states. Strictly speaking, the value of θ defined by Eqs. (29) and (30) is thus not the only satisfying one. Nevertheless, it is the only one for which the equality between $P_E(n_1, n_2)$ and $P'_E(n_1, n_2)$ is systematically satisfied, no matter how close to the most excited states the hypotenuse is. This makes it superior to any other one.

End of additional paragraph 5.

2. Non statistical case

What about non statistical situations ? Given that $\rho(x_1, x_2)$ is non uniform in the energetically allowed triangle, Eq. (33) reads

$$P'_E(n_1, n_2) = \alpha \int_{D_{n_1 n_2}} dy_1 \rho(x_1, x_2). \quad (46)$$

Recall that in the statistical case, the 1GB procedure was justified by the fact that $P'_E(n_1, n_2)$ is equal to $P_E(n_1, n_2)$.

In the present case, $P'_E(n_1, n_2)$ is still a reasonable approximation of $P_E(n_1, n_2)$ provided

that the variation of $\rho(x_1, x_2)$ along the y_1 -axis is sufficiently smooth. If so, it is indeed clear using Eq. (36) that

$$\alpha \int_{D_{n_1 n_2}} dy_1 \rho(x_1, x_2) = \frac{\int_{D_{n_1 n_2}} dy_1 \rho(x_1, x_2)}{\int_{D_{n_1 n_2}} dy_1} \approx \rho(n_1, n_2), \quad (47)$$

the strict equality occurring when $\rho(x_1, x_2)$ varies linearly along the y_1 -axis (and is non zero within $D_{n_1 n_2}$). From Eq. (15), we then arrive at the conclusion that $P'_E(n_1, n_2)$ is roughly equal to $P_E(n_1, n_2)$.

Such a smooth variation of the density in the action space was observed several times in the case of three-atom exchange reactions, the only difference being that the previously introduced x and j actions play the role of x_1 and x_2 . Fig. 4 in reference [20] is a clear illustration of this statement in the case of the direct reaction $O(^3P)+HCl \rightarrow OH+Cl(^2P)$. The energetically available area in the (x, j) plane is given by

$$E \geq \omega(x + \frac{1}{2}) + Bj^2. \quad (48)$$

Its upper limit is thus found to be a curved, instead of straight, line. Moreover, the lines equivalent to the six straight lines in Fig. 1 are also curved. Along these lines (not drawn in Fig. 4 of reference [20]), the density $\rho(x, j)$ evolves rather smoothly. In other words, despite the fact that the distribution of the translational energy is not statistical, the intramolecular vibrational redistribution (IVR) in the strong coupling region tends to distribute in a relatively democratic way the rest of the energy among the vibrational and rotational degrees-of-freedom.

One expects a similar redistribution will also take place among the vibrational modes, due to their couplings. As shown in section IV, this is at least the case for $OH+D_2$ which, as $O(^3P)+HCl$, is a direct process.

F. Collisional system involving three vibrational modes

We now consider the collinear inelastic collision between atom A and the tetra-atomic molecule BCDE involving three vibrational normal modes. Following a reasoning analogous

to the one developed in the previous subsection, we arrived after some steps of algebra to an expression exact (with a Gaussian of zero width) in the statistical limit ($P_E(E_T)$ being still considered as the "exact" density). With $\mathbf{n} = (n_1, n_2, n_3)$, $\mathbf{x} = (x_1, x_2, x_3)$, $D_{\mathbf{n}}$ the unit cube centered on \mathbf{n} , and ω_k, ω_l and ω_m deduced from any cyclic permutation of ω_1, ω_2 and ω_3 , this expression is

$$P_{1GB}(E_T) = \sum_{\mathbf{n}} P_{1GB}(\mathbf{n}) \delta\left(E_T - E + \sum_{i=1}^3 \omega_i(x_i + \frac{1}{2})\right) \quad (49)$$

with

$$P_{1GB}(\mathbf{n}) = \int_{D_{\mathbf{n}}} d\mathbf{x} G\left(\frac{\sum_{i=1}^3 \omega_i(x_i - n_i)}{\omega}\right) \rho(\mathbf{x}), \quad (50)$$

ω being defined as

$$\omega = \frac{\omega_k}{1 - \frac{(\omega_k - \omega_l - \omega_m)^2}{4\omega_l\omega_m}} \quad (51)$$

if $\omega_k < \omega_l + \omega_m$ for the three cyclic permutations, or

$$\omega = \max(\omega_k, \omega_l, \omega_m) \quad (52)$$

if $\omega_k \geq \omega_l + \omega_m$ for only one of the permutations. In the second case, the formulation (see Eqs. (50) and (52)) is a straightforward extension of Eq. (40).

We shall retain from the above developments that for three vibrational modes, the formulation of ω is not unique. It depends on the values of the vibrational frequencies ω_1, ω_2 and ω_3 , contrary to the formulation for two vibrational modes.

Hence, if one does not use the correct expression of ω , one does not find the correct populations. However, the wrong populations turn out to be proportional to the correct ones. The proof is straightforward: if we call ω_c the correct value of ω and ω_w the wrong one, the wrong populations are found from Eqs. (50) (with G replaced by the Dirac distribution) and (19) to be equal to ω_w/ω_c times the correct populations. This explains why the peaks of the 1GB' distribution in Fig. 4 (given by Eqs. (41) and (42)) are $(\omega_1 + \omega_2)/\max(\omega_1, \omega_2)$ higher than the peaks of the 1GB distribution (given by Eqs. (40) and (42)).

We did not extend the above developments in the case of systems involving more than three vibrational modes for the mathematical developments became very tedious. Therefore,

we do not know the analytical expression of ω making the 1GB distribution in close agreement with the "exact" or GB distribution in the statistical limit. However, we go round this difficulty in section II.H.

G. General collisions

The extension of Eq. (6) to a three-dimensional collision involving N vibrational modes is

$$P_C(E_T) = \int dE_R P_C(E_T, E_R) \quad (53)$$

where

$$P_C(E_T, E_R) = \int d\mathbf{x} \rho(\mathbf{x}, E_R) \delta\left(E_T - (E - E_R) + \sum_{i=1}^N \omega_i(x_i + \frac{1}{2})\right), \quad (54)$$

$\mathbf{x} = (x_1, \dots, x_N)$, E_R is the final product rotational energy and $\rho(\mathbf{x}, E_R)$ is the distribution of \mathbf{x} and E_R .

For a given value of E_R , $P_C(E_T, E_R)$ appears to be formally identical to $P_C(E_T)$ in Eq. (6) and consequently, all the developments following Eq. (6) could be repeated here identically. The main conclusion of this section is thus the same as before, i.e., the 1GB procedure leads to nearly the same conclusions as the GB procedure provided that the variation of $\rho(\mathbf{x}, E_R)$ in any plane parallel to the plane

$$E = E_R + \sum_{i=1}^N \omega_n(x_i + \frac{1}{2}) \quad (55)$$

is sufficiently smooth. As stated before, however, we do not know the expressions analogous to Eq. (40) and Eqs. (50)-(52) for N larger than 3.

H. Normalization procedure in realistic calculations

The Monte-Carlo expression of the 1GB populations of the final product quantum states $\mathbf{n} = (n_1, \dots, n_N)$ is given by

$$P_{1GB}(\mathbf{n}) = \frac{1}{N_T} \sum_{k=1}^{N_n} G\left(\frac{\sum_{i=1}^N \omega_i(x_i^k - n_i)}{\omega}\right) \quad (56)$$

where N_T is the total number of trajectories run and $N_{\mathbf{n}}$ is the number of trajectories ending in the product channel with $\mathbf{x} = (x_1, \dots, x_N)$ pointing in $D_{\mathbf{n}}$, the N -dimensional unit cube centered on \mathbf{n} .

As seen before, however, we do not know in the general case the expression of ω leading to 1GB distributions in close agreement with the GB ones in the statistical limit. Nevertheless, the former are proportional to the latter.

One might thus think about re-normalizing 1GB distributions so as to give them the GB norms. But GB norms have no reason to be exactly equal to one, so it is preferable to directly re-normalize 1GB distributions to unity. The corresponding expression is

$$P_{1GB}(\mathbf{n}) = \frac{\sum_{k=1}^{N_{\mathbf{n}}} G\left(\frac{\sum_{i=1}^N \omega_i(x_i^k - n_i)}{\omega}\right)}{\sum_{k=1}^{N_T} G\left(\frac{\sum_{i=1}^N \omega_i(x_i^k - n_i)}{\omega}\right)} \quad (57)$$

where ω may be kept at the maximum of the frequencies or their sum. The final result is not expected to depend significantly on this choice, for it will affect both the numerator and the denominator of Eq. (57) in nearly the same way. This point is illustrated in section IV in the case of the reaction $\text{OH} + \text{D}_2$. Note that in the denominator, the sum is over the whole set of computed trajectories, be they reactive or not. The various quantities in the argument of the Gaussian are thus either those of the products and those of the reformed reagents.

Special care should however be taken with processes involving a large amount of vibrationally elastic non reactive trajectories. Ion-molecule reactions are a typical example. For such processes, an alternative to Eq. (57) is

$$P_{1GB}(\mathbf{n}) = \frac{\min\left[N_{\mathbf{n}}, \sum_{k=1}^{N_{\mathbf{n}}} G\left(\frac{\sum_{i=1}^N \omega_i(x_i^k - n_i)}{\omega}\right)\right]}{\sum_{\mathbf{m}} \min\left[N_{\mathbf{m}}, \sum_{k=1}^{N_{\mathbf{m}}} G\left(\frac{\sum_{i=1}^N \omega_i(x_i^k - m_i)}{\omega}\right)\right]} \quad (58)$$

where the sum over \mathbf{m} in the denominator involves the whole set of final vibrational states, i.e., those of the products as well as those of the reformed reactants. Eq. (58) is a compact form of Eqs. (15) and (16) of reference 23. Eq. (4) of reference 34 may be a second alternative.

III. NON STATISTICAL TEST CASE FOR THREE VIBRATIONAL MODES

We still consider the collinear inelastic collision between atom A and the tetra-atomic molecule BCDE involving three harmonic normal modes. E , ω_1 , ω_2 and ω_3 are respectively kept at 15, 1, 1.7 and 2.9. We also consider the non statistical Gaussian density $\rho(x_1, x_2, x_3)$ given by

$$\rho(x_1, x_2, x_3) = \prod_{i=1}^3 G(x_i - x_i^0) \quad (59)$$

with $x_1^0 = 2.2$, $x_2^0 = 1.3$ and $x_3^0 = 0.7$, ϵ being kept at 0.8 in $G(x_1 - x_1^0)$, 1.4 in $G(x_2 - x_2^0)$ and 0.4 in $G(x_3 - x_3^0)$.

The resulting distributions $P_C(E_T)$, $P_{SB}(E_T)$, $P_{GB}(E_T)$, $P_{1GB}(E_T)$ and $P_E(E_T)$, given by expressions similar to those of the previous section with one more dimension, are represented in Fig. 5. The details of the calculations are exactly the same as in section II.D.1, the only difference being that all the distributions were numerically re-normalized to unity.

Like in the previous statistical example, $P_C(E_T)$ is in poor agreement with $P_E(E_T)$. On the other hand, $P_{GB}(E_T)$ is in very good agreement with $P_E(E_T)$; given the large number of points considered in the Monte-Carlo integration, this is an expected result despite the already "large" number of vibrational modes involved in the collision.

Interestingly, $P_{1GB}(E_T)$ is even in slightly better accord with $P_E(E_T)$ than $P_{GB}(E_T)$ when looking at the details. Such a high level of agreement despite the non-statistical nature of the present process is pleasing. It supports the statement of subsection II.E.2 that for a sufficiently smooth distribution of the final actions, the 1GB procedure represents an accurate alternative to the GB one.

Last but not least, $P_{GB}(E_T)$ does also a good job, though the heights of the peaks corresponding to the largest energies tend to be overestimated.

IV. THE SIMPLEST POLYATOMIC REACTION $\text{OH}+\text{D}_2 \rightarrow \text{HOD}+\text{D}$

This process has been the subject of intense research, both experimentally and theoretically [38–44, 51]. Its mechanism has been well established as being direct, with the products preferentially backward scattered, suggestive of a rebound mechanism. The product trans-

lational energy distribution was experimentally measured by Alagia et al. [38], and by Davis and co-workers four years later [40]. While Alagia et al. found a broad and single-peaked distribution, Davis et al. found a better resolved distribution involving three peaks corresponding to the HOD vibrational states $(n_1, n_2, n_3) = (0,1,0)$, $(0,2,0)$ and $(0,1,1)$. n_1 , n_2 and n_3 are the OH stretching, bending and OD stretching quantum numbers, respectively. This distribution is represented in the top panel of Fig. 6.

In reference 41, 1 000 000 trajectories were run on the Ochoa-Clary (OC) potential energy surface (PES) [51] using the VENUS96 code. Initial conditions were selected to reproduce the experiment of Davis and co-workers, with a collision energy of $6.6 \text{ kcal mol}^{-1}$ and the reactants in their vibrational ground states. The number of reactive trajectories was found equal to $N_P = 10837$. At the end of each reactive trajectory, the vibrational actions of the triatomic HOD product were calculated using the recent normal mode analysis algorithm [52]. The latter includes anharmonicity and Coriolis-coupling terms, and yields results similar to those obtained by means of the widely used fast Fourier transform approach [53], but at a lower computational cost.

The different distributions previously considered are calculated as follows. Formally, the purely classical translational energy distribution is given by Eqs. (53) and (54) with N equal 3. *Stricto-sensu*, its Monte-Carlo expression is

$$P_C(E_T) = \frac{1}{N_T} \sum_{k=1}^{N_T} \delta(E_T - E_T^k) \quad (60)$$

where E_T^k is the final translational energy for the k^{th} trajectory. This energy satisfies the relation

$$E_T^k = E - \sum_{i=1}^3 \omega_i(x_i^k + \frac{1}{2}) - E_R^k, \quad (61)$$

the x_i^k 's and E_R^k being the final vibrational actions and rotational energy for the k^{th} trajectory.

Here, we shall not replace the Dirac distribution in the previous sum by a Gaussian and calculate it for fixed values of E_T . Instead, we divide the available range of energy $[0, E]$ in N_r boxes $[(i-1)E/N_r, iE/N_r]$, $i = \overline{1, N_r}$, and integrate $P_C(E_T)$ over the boxes. This leads

to the N_r populations

$$P_i = \frac{N_i}{N_T}, \quad (62)$$

$i = \overline{1, N_r}$, where N_i is the number of trajectories for which the final translational energy belongs to the i^{th} box.

We note that applying Eq. (60) does only require the calculation of E_T^k , not of x_1^k , x_2^k , x_3^k and E_R^k . On the other hand, the four last quantities are necessary for the calculation of $P_{SB}(E_T)$. This distribution is indeed calculated in the same way as $P_C(E_T)$, the only difference being that the translational energy for the k^{th} trajectory is now given by

$$E_T^k = E - \sum_{i=1}^3 \omega_i(\bar{x}_i^k + \frac{1}{2}) - E_R^k \quad (63)$$

instead of Eq. (61). This difference is similar to the one between Eqs. (6) and (7).

For $P_{GB}(E_T)$, N_i is replaced in Eq. (62) by

$$N_i^{GB} = \sum_{k=1}^{N_i} \prod_{i=1}^3 G(x_i^k - \bar{x}_i^k), \quad (64)$$

the sum being performed over the trajectories for which the final translational energy according to Eq. (61) belongs to the i^{th} box.

For $P_{1GB}(E_T)$, N_i is replaced by

$$N_i^{GB} = \sum_{k=1}^{N_i} G\left(\frac{\sum_{i=1}^3 \omega_i(x_i^k - \bar{x}_i^k)}{\omega}\right), \quad (65)$$

the sum being performed over the same trajectories as above.

Finally, $P_{SB}(E_T)$, $P_{GB}(E_T)$ and $P_{1GB}(E_T)$ were re-normalized to one. ϵ was kept at 0.05 for $P_{GB}(E_T)$, and 0.01 for $P_{1GB}(E_T)$. ω was identified with the largest frequency. The distributions are displayed in Fig. 6. We also kept ω at the sum of the frequencies, following Czako and Bowman [37], but due to the re-normalization, this left the distribution unchanged.

Contrary to the purely classical distribution which has a bell shape and does not reproduce the vibrational structures observed experimentally [43, 44], the SB, GB and 1GB distributions reproduce quite satisfyingly the two structures due to the (0,1,0) and (0,2,0) vibrational states. On the other hand, the third structure, due to the (0,1,1) state, is strongly underestimated by all the treatments. Comparison with exact quantum scattering calculations, certainly possible in a near future, will tell if the previous disagreement is due to possible inaccuracies of the OC-PES or to the present classical descriptions.

The SB procedure does a good job, though it overestimates the contribution of the small translational energies to the (0,2,0) peak.

The GB distribution of Fig. 6 involves strong fluctuations, contrary to the same density represented in Fig. 2 of reference 41. The reason is that in the present work, we did not use the smoothing procedure previously considered [44] (two Gaussian functions were used to fit the left and right-hand side of each vibrational contribution). We did it on purpose, in order to illustrate the fact that with ~ 11000 reactive trajectories and three vibrational modes, the usual GB procedure generates quite noisy curves. On the other hand, the 1GB distribution is much better converged and one guesses that it represents the curve one would obtain from smoothing the GB curve.

Owing to the fact that the OH+D₂ reaction is a direct process, the present results are quite encouraging for future applications of the 1GB procedure to polyatomic reactions, do they involve a long-lived complex or not.

V. CONCLUSION

In the recent years, many processes have been studied by the quasi-classical trajectory method (QCTM) within the Gaussian binning (GB) procedure. In most studies, the population of the final product quantum state $\mathbf{n} = (n_1, \dots, n_N)$, N being the number of quantized degrees of freedom (DOF), was approximated by

$$P_{\mathbf{n}} = \frac{1}{N_T} \sum_{k=1}^{N_{\mathbf{n}}} \prod_{i=1}^N G(x_i^k - n_i) \quad (66)$$

instead of the usual expression

$$P_{\mathbf{n}} = \frac{N_{\mathbf{n}}}{N_T} \quad (67)$$

used in the standard binning (SB) procedure (or histogram method). N_T is the total number of trajectories run, $\mathbf{x} = (x_1, \dots, x_N)$ is the final action state, $N_{\mathbf{n}}$ is the number of trajectories ending in the product channel with \mathbf{x} pointing in the N -dimensional unit cube centered on \mathbf{n} and G is a Gaussian normalized to unity, with a full width at half maximum of ~ 10 percent.

Since most processes studied so far by GB-QCTM were triatomic reactions, one single vibrational DOF was quantized, meaning that the Gaussian product in Eq. (66) reduced to one term only. As about 10 percent of the total amount of reactive trajectories do actually contribute to the product populations, 10 times more trajectories had to be run for keeping with the same level of convergence of the predictions as compared with SB-QCTM.

Nowadays, however, more and more processes under scrutiny involve more than one vibrational mode. For instance, the reaction $\text{OH} + \text{D}_2 \rightarrow \text{HOD} + \text{D}$ involves three modes while for the reaction $\text{F} + \text{CH}_4 \rightarrow \text{FH} + \text{CH}_3$, this number is seven. Consequently, GB-QCTM requires one thousand more trajectories than SB-QCTM for the first process and ten millions more for the second ! It is thus quite clear that as such, Eq. (66) has no future in the area of polyatomic reaction dynamics.

This is why Czako and Bowman [37] recently proposed to "quantize" the total vibrational energy instead of the vibrational actions, introducing the expression

$$P_{\mathbf{n}} = \frac{1}{N_T} \sum_{k=1}^{N_{\mathbf{n}}} G\left(\frac{\sum_{i=1}^N \omega_i (x_i^k - n_i)}{\omega}\right) \quad (68)$$

where ω_i is the i^{th} normal mode frequency and

$$\omega = \sum_{i=1}^N \omega_i. \quad (69)$$

The key feature of this *ad-hoc* quantization as compared to the previous one-Gaussian-for-one-mode approach is that only one Gaussian function is used whatever the number of vibrational DOF of the system, a huge amount of computational time being therefore saved. We called it the 1GB procedure.

The conclusions of the present paper are as follows:

- 1) For a statistical collision involving two product vibrational modes, the 1GB procedure is strictly equivalent to the GB procedure provided that ω is identified with the maximum of the ω_i 's instead of their sum.
- 2) For a statistical collision involving three product vibrational modes, the 1GB procedure is strictly equivalent to the GB procedure provided that ω is kept at the maximum frequency in part of the frequency space, and a more complex expression (see Eq. (51)) in the remaining part.
- 3) For the previous processes and a non statistical but sufficiently smooth distribution in the action space, the 1GB procedure leads to results in satisfying agreement with the GB ones.
- 4) Finding the expression of ω for any realistic process involving more than three product vibrational modes requires heavy mathematical developments that we did not perform. However, one may go round this difficulty by re-normalizing the product state populations. In such a case, ω can be indifferently kept at the maximum of the ω_i 's or their sum. Special care should however be taken with processes involving a large amount of vibrationally elastic non reactive trajectories, like ion-molecule reactions. The methods proposed in reference 23 (leading to Eq. (58) of the present work) or 34 can then be used.
- 5) The 1GB procedure leads to results in good agreement with the GB one for (a) a non statistical test case involving three vibrational modes and (b) the prototype four-atom reaction $\text{OH} + \text{D}_2 \rightarrow \text{HOD} + \text{D}$.

In conclusion, the 1GB procedure might be of great interest for future classical simulations of polyatomic chemical reaction dynamics in the highly quantum mechanical situation where only a few product vibrational states are available.

Appendix

Consider (i) the N -dimensional space $\mathbf{\Gamma} = (x_1, \dots, x_N)$, (ii) a given distribution $\rho(\mathbf{\Gamma})$, normalized to unity, of the position in the previous space and (iii) the quantity Q' depending on $\mathbf{\Gamma}$ according to

$$Q' = f(\mathbf{\Gamma}). \quad (\text{B.1})$$

The probability that Q' is lower than a given value Q is given by

$$\Pi(Q) = \int d\mathbf{\Gamma} \rho(\mathbf{\Gamma}) \Theta(Q - Q') = \int d\mathbf{\Gamma} \rho(\mathbf{\Gamma}) \Theta(Q - f(\mathbf{\Gamma})) \quad (\text{B.2})$$

where $\Theta(x)$ is the Heaviside function, equal to 0 for x negative and 1 in the contrary case. $\Theta(Q - Q')$ ensures that integration with respect to $\mathbf{\Gamma}$ is made over the volume such that Q minus Q' is positive, i.e., Q' is lower than Q .

If $P(Q)$ is the density of probability that Q' takes the value Q , $P(Q)dQ$ is the probability that Q' belongs to the range $[Q, Q + dQ]$. We then have

$$P(Q)dQ = \Pi(Q + dQ) - \Pi(Q) \quad (\text{B.3})$$

that is,

$$P(Q) = \frac{d\Pi}{dQ}. \quad (\text{B.4})$$

From Eq. (B.2), we finally arrive at

$$P(Q) = \int d\mathbf{\Gamma} \rho(\mathbf{\Gamma}) \delta(Q - f(\mathbf{\Gamma})), \quad (\text{B.5})$$

as the Dirac distribution $\delta(x)$ is the first derivative of $\Theta(x)$. Eq. (6) is straightforwardly obtained from Eqs. (B.5), (4) and (5).

Acknowledgments

LB is indebted to Pr. J.-C. Rayez for careful reading of the manuscript prior to its publication as well as stimulating discussions on its content and more generally, on the semi-classical description of molecular collisions.

-
- [1] R. Levine, *Molecular Reaction Dynamics*, Cambridge University Press, 2005.
- [2] See, among many others, I. N. Levine, *Quantum Chemistry*, 6th Edition, Prentice Hall, 2008 ; F. L. Pilar, *Elementary Quantum Chemistry*, Second Edition, Dover Publications, 2001 ; T. Helgaker, P. Jorgensen and J. Olsen, *Molecular Electronic Structure Theory*, Wiley, 2000.
- [3] P. Honvault and J.-M. Launay in *Theory of Chemical Reaction Dynamics*, Kluwer Academic Publishers, 2004.
- [4] V. Aquilanti and S. Tonzani, *J. Chem. Phys.*, 120, 4066 (2004).
- [5] G. Nyman and H.-G. Yu, *Rep. Prog. Phys.*, 63, 1001 (2000).
- [6] S. Althorpe in *The Encyclopedia of Computational Chemistry*, Ed. P. Schleyer, Wiley, Athens, 2005.
- [7] W. Hu and G. C. Schatz, *J. Chem. Phys.*, 125, 132301 (2006).
- [8] B. Lepetit, D. Wang and A. Kuppermann, *J. Chem. Phys.*, 125, 133505 (2006).
- [9] X.Q. Zhang, Q. Cui, J.Z.H. Zhang, K.L. Han, *J. Chem. Phys.*, 126, 234304 (2007).
- [10] D. De Fazio, V. Aquilanti, S. Cavalli, A. Aguilar and J. M. Lucas, *J. Chem. Phys.*, 129, 064303 (2008).
- [11] R. N. Porter and L. M. Raff, in *Dynamics of molecular collisions*, Part B, edited by W. H. Miller, Plenum, New York, 1976.
- [12] T. D. Sewell and D. L. Thomson, *Int. J. Mod. Phys. B*, 11, 1067 (1997).
- [13] D. Clary, *Phys. Chem. Chem. Phys.*, 9, pp.C21 (2007) and references therein.
- [14] M. Ragni, A. C. P. Bitencourt and V. Aquilanti, *Int. J. Quant. Chem.*, 107, 2870 (2007).
- [15] B. Lepetit, D. Wang and A. Kuppermann, *J. Chem. Phys.*, 125, 133505 (2006).
- [16] S. Schmatz, *ChemPhysChem*, 5, 600 (2004).
- [17] M. Yang, S-Y. Lee, and D. H. Zhang *J. Chem. Phys.*, 126, 064303 (2007).
- [18] L. Bonnet and J.-C. Rayez, *Chem. Phys. Lett.*, 277, 183 (1997).
- [19] L. Bañares, F. J. Aoiz, P. Honvault, B. Bussery-Honvault and J.-M. Launay, *J. Chem. Phys.*, 118, 565 (2003).
- [20] T. Xie, J. Bowman, J. W. Duff, M. Braunstein and B. Ramachandran *J. Chem. Phys.*, 122, 014301 (2005).
- [21] M. L. González-Martínez, L. Bonnet, P. Larrégaray and J.-C. Rayez, *J. Chem. Phys.*, 126,

- 041102 (2007).
- [22] S. Ron, M. Baer and E. Pollak, *J. Chem. Phys.*, 78, 4414 (1983).
- [23] L. Bonnet and J.-C. Rayez, *Chem. Phys. Lett.*, 397, 106 (2004).
- [24] L. Bonnet, *J. Chem. Phys.*, 128, 044109 (2008).
- [25] W. H. Miller, *J. Chem. Phys.*, 53, 1949 (1970).
- [26] R. A. Marcus, *Chem. Phys. Lett.*, 7, 252 (1970).
- [27] W. H. Miller, *Adv. Chem. Phys.*, 25, 69 (1974).
- [28] W. H. Miller, *J. Phys. Chem. A*, 105, 2942 (2001).
- [29] M. S. Child, *Molecular Collision Theory*, 1974 (Academic Press).
- [30] J. N. L. Connor, *Chem. Soc. Rev.*, 5, 125 (1976).
- [31] L. Bonnet and C. Crespos, *Phys. Rev. A*, 78, 062713 (2008).
- [32] Z. Sun, D. H. Zhang, C. Xu, S. Zhou, D. Xie, G. Lendvay, S-Y. Lee, S. Y. Lin, and H. Guo, *J. Am. Chem. Soc.*, 130, 14962 (2008).
- [33] G. Lendvay, D. Xie and H. Guo, *Chem. Phys.*, 349, 181 (2008).
- [34] P. Halvick, T. Stoecklin, P. Larrégaray and L. Bonnet, *Phys. Chem. Chem. Phys.*, 9, 582 (2007).
- [35] Z. Sun, L. Liu, S.Y. Lin, R. Schinke, H. Guo, D.H. Zhang, *Proc. Nat. Acad. Sci.*, 107, 555 (2010).
- [36] K. Liu, *Phys. Chem. Chem. Phys.*, 9, 17 (2007).
- [37] G. Czako and J. M. Bowman, *J. Chem. Phys.*, 131, 244302 (2009).
- [38] M. Alagia, N. Balucani, P. Casavecchia, D. Stranges, G. G. Volpi, D. C. Clary, A. Kliesch and H.-J. Warner, *Chem. Phys.*, 207, 389 (1996).
- [39] S. K. Pogrebnya, J. Palma, D. C. Clary and J. Echave, *Phys. Chem. Chem. Phys.*, 2000, 2, 693, *Phys. Chem. Chem. Phys.*, 2, 693 (2000).
- [40] B. R. Strazisar, C. Lin and H. F. Davis, *Science*, 290, 958 (2000).
- [41] J. D. Sierra, P. A. Enriquez, D. Troya and M. Gonzalez, *Chem. Phys. Lett.*, 399, 527 (2004).
- [42] E. Garcia, A. Saracibar, A. Rodríguez, A. Lagana and G. Lendvay, *Mol. Phys.*, 2006, 104, 839 *Mol. Phys.*, 104, 839 (2006).
- [43] J. D. Sierra, R. Martínez, J. Hernando and M. González, *Phys. Chem. Chem. Phys.*, 11, 11520 (2009).
- [44] J. Espinosa-Garcia, L. Bonnet and J. C. Corchado, *Phys. Chem. Chem. Phys.*, 12, 3873 (2010).

- [45] L. Bonnet and J.-C. Rayez, *J. Phys. Chem. A*, 101, 9318 (1997).
- [46] P. Larrégaray, L. Bonnet and J.-C. Rayez, *J. Phys. Chem. A*, 110, 1552 (2006).
- [47] L. Bonnet, P. Larrégaray, J.-C. Rayez and T. Gonzalez-Lezana, *Phys. Chem. Chem. Phys.*, 8, 3951 (2006).
- [48] T. González-Lezana, *Int. Rev. Phys. Chem.*, 26, 29 (2007).
- [49] F. J. Aoiz, V. S Rábanos, T. González-Lezana and D. E. Manolopoulos, *J. Chem. Phys.*, 126, 161101 (2007).
- [50] L. Bonnet, P. Larrégaray and J.-C. Rayez, *Phys. Chem. Chem. Phys.*, 9, 3228 (2007).
- [51] G. Ochoa de Aspuru and D. Clary, *J. Phys. Chem. A*, 102, 9631 (1998)
- [52] J. C. Corchado and J. Espinosa-Garcia, *Phys. Chem. Chem. Phys.*, 11, 10157 (2009).
- [53] G. C. Schatz, *Comput. Phys. Commun.*, 51, 135 (1988).

Figures captions

Fig. 1: The action space defined by Eq. (17) and both x_1 and x_2 greater than minus 1/2 is represented here by a green triangle while the available quantum states are represented by six red dots. The distribution of the action pair (x_1, x_2) is uniform in the triangle. Each dot lies along a straight-line corresponding to a given translational energy (see Eq. (25)). Three forbidden quantum states are represented by dark blue dots and three unit squares centered on quantum states are emphasized. The two salmon ones correspond to available quantum states while the light blue one corresponds to a forbidden state.

Fig. 2: Translational energy distributions corresponding to the statistical distribution in the green triangle of Fig. 1. The curves are labeled by the subscript of their mathematical symbols (see text). The distributions are not normalized to unity.

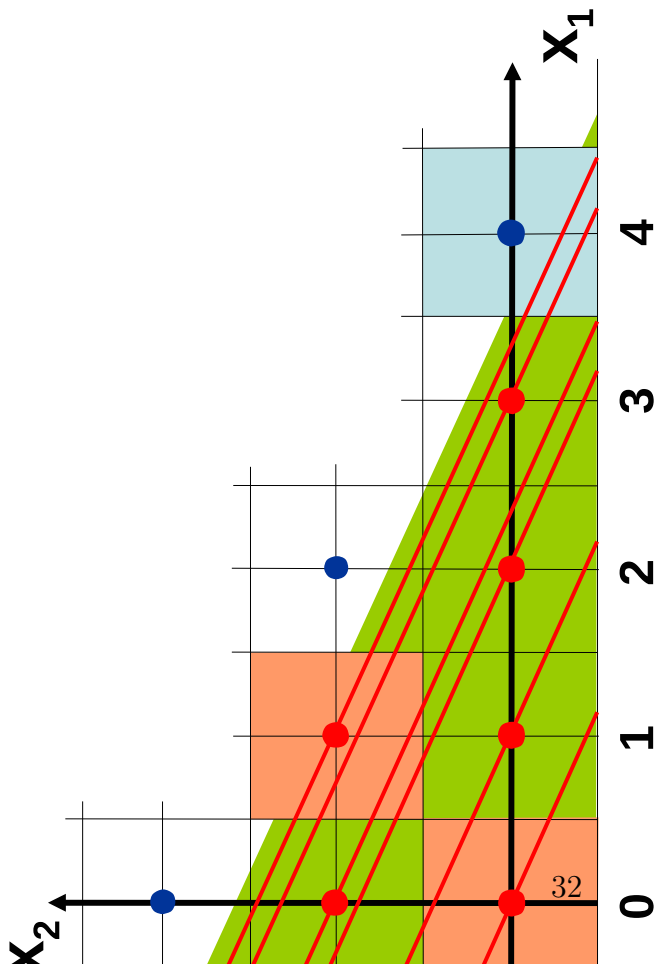
Fig. 3: Drawing shedding light on the derivation of Eq. (40). $\cos\theta$ clearly appears to be the reciprocal of the section of the new coordinate axis y_1 being within the red square (see Eq. (34)).

Fig. 4: Translational energy distributions corresponding to the statistical distribution in the green triangle of Fig. 1. The curves are labeled by the subscript of their mathematical symbols (see text). The distributions are not normalized to unity.

Fig. 5: Translational energy distributions corresponding to the non statistical distribution given by Eq. (59). The curves are labeled by the subscript of their mathematical symbols (see text). The distributions are not normalized to unity.

Fig. 6: Translational energy distributions in the products of the reaction $\text{OH} + \text{D}_2 \rightarrow \text{HOD} + \text{D}$ studied at the conditions of the group of Davis [40]. The top curve is the experimental distribution while the remaining curves are labeled by the subscript of their mathematical symbols (see text). The distributions are normalized to unity.

Figures



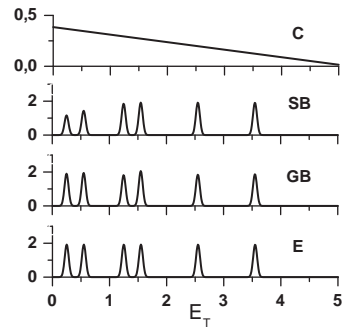


Figure 2:

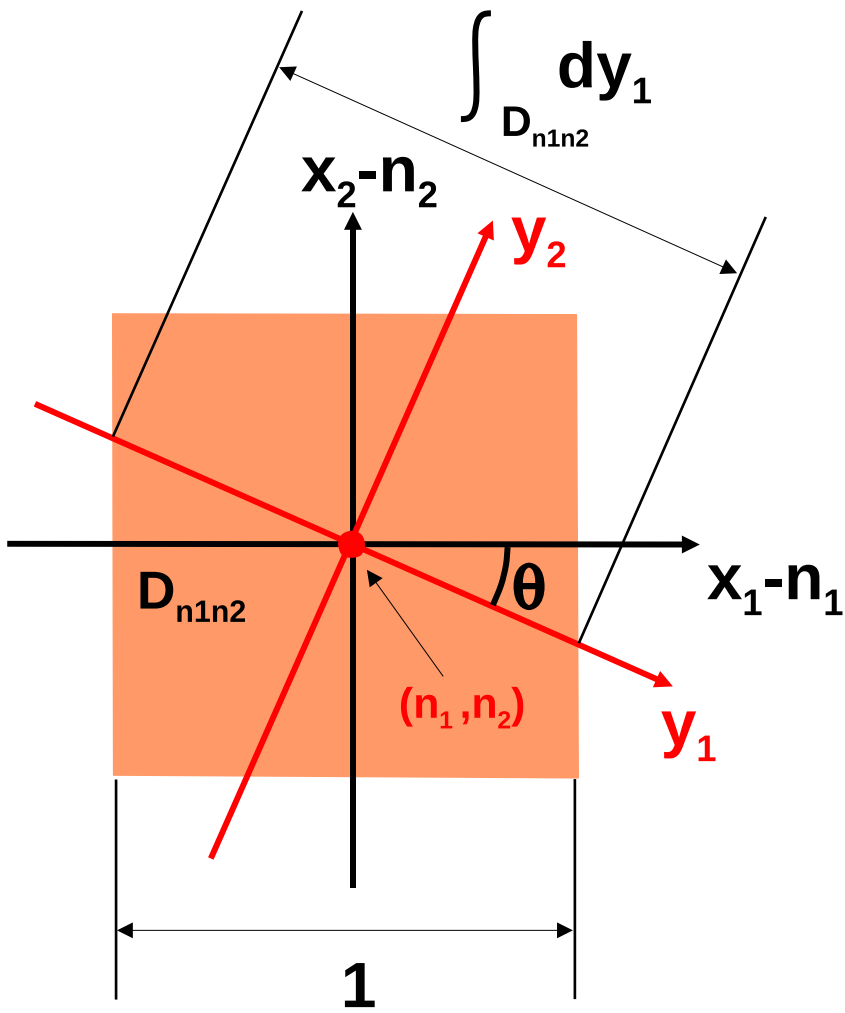


Figure 3:

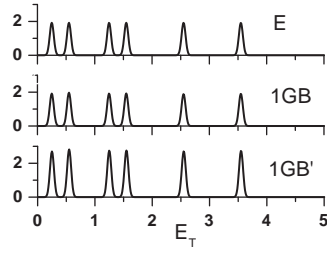


Figure 4:

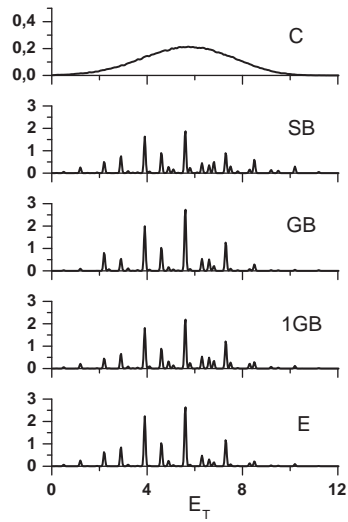


Figure 5:

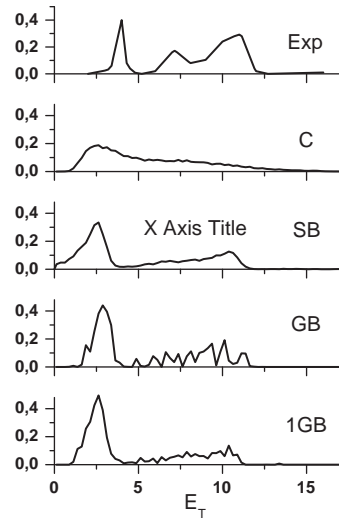


Figure 6: